Biochimica et Biophysica Acta 1852 (2015) 1561–1573

Contents lists available at ScienceDirect

Biochimica et Biophysica Acta

journal homepage: www.elsevier.com/locate/bbadis

# Sequence-dependent abnormal aggregation of human Tau fragment in an inducible cell model

Xiao-Ling Liu [a], Ji-Ying Hu [a], Meng-Yun Hu [a], Yi Zhang [a], Zheng-Yuan Hong [b], Xiao-Qing Cheng [a], Jie Chen [a], Dai-Wen Pang [b], Yi Liang [a,*]

[a] State Key Laboratory of Virology, College of Life Sciences, Wuhan University, Wuhan 430072, China
[b] College of Chemistry and Molecular Sciences, State Key Laboratory of Virology, Wuhan University, Wuhan 430072, China

ARTICLE INFO

*Article history:*
Received 24 November 2014
Received in revised form 27 March 2015
Accepted 14 April 2015
Available online 22 April 2015

*Keywords:*
Tau protein
Alzheimer disease
Fibril-forming motif
Protein aggregation
Apoptosis

ABSTRACT

A pathological hallmark of Alzheimer disease (AD) is the accumulation of misfolded hyperphosphorylated microtubule-associated protein Tau within neurons, forming neurofibrillary tangles and leading to synaptic dysfunction and neuronal death. Here we study sequence-dependent abnormal aggregation of human fragment $Tau_{244–372}$ in an inducible cell model. As evidenced by confocal laser scanning microscopy, Western blot, and immunogold electron microscopy, fibril-forming motifs are essential and sufficient for abnormal aggregation of $Tau_{244–372}$ in SH-SY5Y neuroblastoma cells induced by Congo red: when its two fibril-forming segments PHF6 and PHF6* are deleted, $Tau_{244–372}$ does lose its ability to form fibrils in SH-SY5Y cells, and the replacement of PHF6 and PHF6* with an unrelated amyloidogenic sequence IFQINS from human lysozyme does rescue the fibril-forming ability of $Tau_{244–372}$ in SH-SY5Y cells. By contrast, insertion of a non-fibril forming peptide GGGG GG does not drive the disabled $Tau_{244–372}$ to misfold in SH-SY5Y cells. Furthermore, as revealed by quantum dots based probes combined with annexin V staining, annexin V-FITC apoptosis detection assay, and immunofluorescence, fibril-forming motifs are essential and sufficient for early apoptosis of living SH-SY5Y cells induced by abnormal aggregation of $Tau_{244–372}$. Our results suggest that fibril-forming motifs could be the determinants of Tau protein tending to misfold in living cells, thereby inducing neuronal apoptosis and causing the initiation and development of AD.



## 1. Introduction

A pathological hallmark of Alzheimer disease (AD) and Pick disease is the accumulation of misfolded hyperphosphorylated microtubule-associated protein Tau within neurons, forming neurofibrillary tangles and leading to synaptic dysfunction and neuronal death [1–5]. AD and Pick disease are progressive and irreversible neurodegenerative diseases caused by the fibrillization of human Tau protein in cells [5], and have posed a serious threat to human health. The most important 125 scientific questions we want to address in the next 100 years have been put forward in *Science* nine years ago, one of which is "to what extent can we stave off Alzheimer disease?" [6]. There is no efficient treatment available for AD and Pick disease and their mechanism is not well understood so far [5]. Thus the characterization of factors regulating Tau protein fibrillization is of great importance to clarify the etiology of AD and Pick disease and to assist in the establishment of medical treatment [7–12].

What are the key factors causing more than 20 amyloidogenic proteins to misfold in cells, thereby leading to numerous neurodegenerative diseases? The Eisenberg lab has provided the first demonstration that fibril-forming motifs identified from amyloidogenic proteins form the core of amyloid fibrils [13,14], and has developed a structure-based, computational approach to identifying these motifs [15]. Such fibril-forming segments themselves can form amyloid fibrils *in vitro*, their atomic structures reveal tightly packed β-sheets with steric zipper interfaces characteristic of the amyloid state [13,14], and they can force a non-fibrillizing protein to form amyloid fibrils [16]. Furthermore, the Eisenberg lab has recently used the atomic structures of fibril-forming motifs as templates, designed an all-D-amino-acid inhibitor of Tau fibrillization [17], and found that amyloid β-sheet mimics containing fibril-forming segments can inhibit the aggregation of amyloidogenic proteins and reduce amyloid toxicity [18]. Although it has been previously demonstrated that two fibril-forming motifs $^{275}$VQIINK$^{280}$ (PHF6*) and $^{306}$VQIVYK$^{311}$ (PHF6) are essential and sufficient for the fibrillization of human Tau *in vitro* [19–21], we do not know whether such motifs are also important for abnormal aggregation of human Tau protein *in vivo* and thereby induce AD and Pick disease.

*Abbreviations:* AD, Alzheimer disease; TEM, transmission electron microscopy; ThT, thioflavin T; Q-dots, quantum dots; DTT, dithiothreitol; PI, propidium iodide

* Corresponding author at: State Key Laboratory of Virology, College of Life Sciences, Wuhan University, Wuhan 430072, China. Tel./fax: +86 27 68754902.
*E-mail address:* liangyi@whu.edu.cn (Y. Liang).

http://dx.doi.org/10.1016/j.bbadis.2015.04.015
0925-4439/

Human Tau fragment $Tau_{244–372}$ contains the four-repeat microtubule binding domain of human Tau forming the core of neurofibrillary tangles in AD, and can form fibrils with the help of the polyanion inducer heparin *in vitro* in a relatively short time [8–10,17,19–24]. Anionic dyes such as Congo red are also able to induce Tau fibrillization *in vitro*[25,26]. Furthermore, Congo red has been used to induce abnormal aggregation of human Tau protein in both HEK-293 cells and SH-SY5Y neuroblastoma cells [26,27].

Semiconductor quantum dots (Q-dots), with high broad excitation spectra, high brightness, superior photostability, resistance to photobleaching, and non-toxicity, have fascinated biologists over the last few years as optical labeling nanomaterials [28,29]. Atomic identification of fluorescent Q-dots on Tau-positive fibrils in 3D-reconstructed Pick bodies has been reported recently [30].

In this study, we firstly studied sequence-dependent abnormal aggregation of human Tau protein in an inducible cell model by using Congo red as the agonist. Congo red, an aromatic heterocycle, is capable of inducing Tau fibrillization both *in vitro* and *in vivo* for its transmembrane property [25–27]. Therefore, we built an inducible cell model to demonstrate for the first time that fibril-forming motifs are essential and sufficient for the fibrillization of human $Tau_{244–372}$ in SH-SY5Y cells by using Congo red binding assays, confocal laser scanning microscopy, transmission electron microscopy (TEM), and immunogold electron microscopy. Furthermore, insertion of a fibril-forming peptide IFQINS from human lysozyme (an aggregation competent motif [13,15]) did drive but insertion of non-fibril forming peptide GGGGGG (an aggregation incompetent motif [16]) did not drive the disabled $Tau_{244–372}$ to form fibrils in SH-SY5Y cells, implicating that fibril-forming motifs could be the determinants of Tau protein tending to misfold *in vivo*, thereby causing the initiation and development of AD and Pick disease. We thus suggest that sequence-dependent aggregation could be a key mechanism for the misfolding of many amyloidogenic proteins.

## 2. Materials and methods

### 2.1. Materials

Congo red (fresh molecular weight of 696.67), thioflavin T (ThT), and thioflavin S (ThS) were from Sigma-Aldrich (St. Louis, MO). Dithiothreitol (DTT) was obtained from Amresco (Solon, OH). DNA polymerase Kod-plus-Neo was from Toyobo (Tokyo, Japan). Anti-FLAG monoclonal antibody and 10-nm gold-labeled anti-mouse antibody were purchased from Sigma-Aldrich (St. Louis, MO). Mouse anti-Tau (TAU-5) monoclonal antibody was Santa Cruz Biotechnology products (Santa Cruz, CA). Alexa 546-conjugated goat anti-mouse IgG secondary antibody was from Invitrogen (Carlsbad, CA). Other chemicals used were made in China and of analytical grade.

### 2.2. Plasmids and proteins

The construction of prokaryotic plasmid expressing $Tau_{244–372}$ and its mutants, and Tau protein purification were carried as described [8–10,19].

### 2.3. Cell culture and transfection

SH-SY5Y neuroblastoma cells were cultured in Dulbecco's modified Eagle's medium supplemented with 10% (v/v) fetal bovine serum (FBS), 100 U/ml penicillin, and 100 U/ml streptomycin in 5% $CO_2$ at 37 °C. SH-SY5Y cells were transiently transfected with FLAG-tagged human Tau in pCMV-Tag 2B vector using Lipofectamine® 2000 (Invitrogen, Carlsbad, CA) according to the manufacturer's protocol.

### 2.4. Plasmid and stable cell line construction

SH-SY5Y cell line stably expressing FLAG-tagged human $Tau_{244–372}$ΔK280 (stable $Tau_{244–372}$ΔK280-FLAG cells) was constructed with lentiviral vector construction system. Human $Tau_{244–372}$ΔK280 was cloned into a lentiviral vector pHAGE-puro by Mlu I and BamH I restriction sites. Lentiviral vector construction system constructed with CMV promoter was packaged in HEK293T cells by various combinations of plasmids and liposome, the three plasmids pHAGE-$Tau_{244–372}$ΔK280, pVSVG, and pLP were mixed at a ratio of 2:1:1 and the ratio of liposome to DNA was 2:1. After 36 h transfection, we harvested the virus, and then SH-SY5Y cells were infected by the packaged lentivirus with a high infection efficiency detected by Western blot.

### 2.5. Congo red binding assays

A stock solution of 200 μM Congo red was prepared in 10 mM HEPES buffer (pH 7.4) containing 100 mM NaCl. This solution was filtered through a 0.22 μm pore size filter before use 5 μM Tau protein (wild-type $Tau_{244–372}$ and its mutants) was incubated in 10 mM HEPES buffer (pH 7.4) containing 2 mM DTT and 100 mM NaCl in the presence of 50 μM Congo red, and Tau aggregation analysis *in vitro* was carried out at 37 °C. To mimic the reducing environment present in normal neuronal cells and block the formation of an intramolecular disulfide bond in Tau protein, 2 mM DTT was added into the buffer. The ultraviolet absorbance spectra of such Tau aggregation induced by Congo red were set up by a mixture of 5 μM Tau protein and 50 μM Congo red in 10 mM HEPES buffer. The reaction components were mixed quickly and read for 0 and 12 h at 37 °C, recording the absorbance spectra from 650 nm to 400 nm on a UV-2550 Probe spectrophotometer (Shimadzu, Kyoto, Japan).

The polymerization induced by Congo red for $Tau_{244–372}$ in 96-well plates was set up by a mixture of 10 μM Tau protein, in the presence of 0, 5, 10, 20, 50, 80, 100 and 150 μM Congo red in 10 mM HEPES buffer containing 2 mM DTT and 100 mM NaCl (pH 7.4). The reaction components were mixed quickly and immediately read for 10 h at 37 °C in a SpectraMax M2 microplate reader (Molecular Devices, Sunnyvale, CA) using absorbance at 550 nm. Each sample was run in triplicate.

Kinetic parameters were determined by fitting the absorbance at 550 nm *versus* time to a sigmoidal equation [8,9,31,32],

$$A = A_0 + (B + ct)/\{1 + \exp[k(t_m - t)]\} \quad (1)$$

where $A$ is the absorbance at 550 nm, $k$ the rate constant for the growth of fibrils, and $t_m$ the time to 50% of maximal absorbance at 550 nm. $A_0$ describes the initial baseline during the lag time. $B + ct$ describes the final baseline after the growth phase has ended. The lag time is determined to be $t_m - 2 / k$.

### 2.6. Transmission electron microscopy (TEM)

The formation of fibrils by $Tau_{244–372}$ and its mutants induced by Congo red was confirmed by electron microscopy of negatively stained samples. Sample aliquots of 10 μl were placed on carbon-coated copper grids (Shanghai Mainstream Trading Company, Shanghai, China), and left at room temperature for 1–2 min, rinsed with $H_2O$ twice, and then stained with 2% (w/v) uranyl acetate for another 1–2 min. The stained samples were examined using an H-8100 transmission electron microscope (Hitachi, Tokyo, Japan) operating at 100 kV or an FEI Tecnai G2 20 transmission electron microscope (Hillsboro, OR) operating at 200 kV.

### 2.7. Laser scanning confocal analysis

SH-SY5Y cells transiently over-expressing FLAG-tagged wild-type $Tau_{244–372}$, $Tau_{244–372}$/ΔPHF6/ΔPHF6* inserted by IFQINS, $Tau_{244–372}$/ΔPHF6 (PHF6-deleted mutant), $Tau_{244–372}$/ΔPHF6* (PHF6*-deleted mutant), $Tau_{244–372}$/ΔPHF6/ΔPHF6*, $Tau_{244–372}$/ΔPHF6/ΔPHF6* inserted

by GGGGGG were incubated with 10 μM Congo red as follows: SH-SY5Y cells were cultured in medium containing 10 μM Congo red for 3 days, planted onto the coverslips in the presence of 10 μM Congo red for 3 days, and then transfected with plasmids transiently. After 48 h, cells were fixed with paraformaldehyde, ruptured with 0.25% Triton-X 100, stained with 250 μM ThT, coimmunostained with primary monoclonal antibodies Anti-FLAG and secondary Alexa Fluo-546, and visualized by confocal microscopy. $Tau_{244–372}$ΔK280 stably expressed in SH-SY5Y cells formed aggregates in the cells in the absence of Congo red. SH-SY5Y cell line stably expressing human $Tau_{244–372}$ΔK280 tagged with FLAG (stable $Tau_{244–372}$ΔK280-FLAG cells) was grown on glass coverslips for 5 days and analyzed for protein aggregation. For confocal microscopy analysis, cells were fixed with paraformaldehyde, ruptured with 0.25% Triton-X 100, stained with 0.1% ThS, coimmunostained with primary monoclonal antibodies Anti-FLAG or TAU-5 and secondary Alexa Fluo-546, and visualized by confocal microscopy. Images were captured using an Olympus FluoView FV1000 laser scanning confocal microscope (Tokyo, Japan). Green fluorescence was detected using the 488-nm laser line of an Argon laser, and red fluorescence was detected using the 559-nm laser line of the HeNe laser.

SH-SY5Y cells were incubated with Q-dots labeled Tau or Q-dots alone in Opti-MEM culture medium for 4 h. After 4 h, SH-SY5Y cells were washed with PBS buffer twice and incubated with a fresh cell culture medium. Olympus FluoView FV1000 fluorescence microscope was then used to observe Q-dots in living SH-SY5Y cells.

### 2.8. Western blot

SH-SY5Y cells were cultured in medium containing 10 μM Congo red for 3 days, planted onto the coverslips in the presence of 10 μM Congo red for 3 days, and then transfected with plasmids transiently. After 48 h, cells were harvested, half was lysed, and then separated into supernatant and pellet fractions by ultracentrifugation at 15,000 *g* for 20 min, while the other half was lysed to get whole cell lysis buffer. Whole cell lysis buffer and ultracentrifugation pellets were boiled in SDS-PAGE loading buffer, respectively, subjected to 13.5% SDS-PAGE and transferred onto polyvinylidene difluoride membranes (Millipore, Billerica, MA), and blocked with 5% fat-free milk in 25 mM Tris buffered saline buffer mixed with 0.047% Tween 20. Western blot of whole cell lysis buffer was carried out by using monoclonal anti-FLAG primary antibody (Sigma-Aldrich) at a dilution of 1:1000 and anti-actin primary antibody (BeyoECL Plus, Beyotime, Nantong, China) at a dilution of 1:1000 separately, followed by goat anti-mouse horseradish peroxidase-conjugated secondary antibody at a dilution of 1:2000. Western blot of pellets was carried out by using monoclonal anti-FLAG primary antibody at a dilution of 1:1000, followed by goat anti-mouse horseradish peroxidase-conjugated secondary antibody at a dilution of 1:2000. Immunoreactive bands were visualized using enhanced chemiluminescence (BeyoECL Plus, Beyotime, Nantong, China).

### 2.9. Immunoelectron microscopy

SH-SY5Y cells were homogenized in ice-cold buffer H (10 mM Tris–HCl, 1 mM EGTA, 0.8 M NaCl, 10% sucrose and protease inhibitor mixture, pH 7.4), and centrifuged for 20 min at 20,000 *g*. Pellet fractions were discarded, while supernatant fractions (S1) were saved and incubated with 1% Sarkosyl for half an hour at room temperature with agitation. After centrifugation of the mixture (1 h at 100,000 *g*), the resultant pellets were re-suspended in 30 mM Tris–HCl (pH 7.4). Aliquots were absorbed onto Formvar/carbon-coated grids and incubated with the Anti-FLAG monoclonal antibody (primary antibody) for 30 min at 37 °C. After washing with 0.1% bovine serum albumin, grids were incubated with the 10-nm gold-labeled goat anti-mouse monoclonal antibody (secondary antibody). Samples were then stained with 2% uranyl acetate for 1 min, and viewed by electron microscopy (Hillsboro, OR).

### 2.10. Quantum dots based probes combined with Annexin V staining

SH-SY5Y cells were cultured in medium containing 10 μM Congo red for 7 days, planted onto the mini-dishes in the presence of 10 μM Congo red overnight. Q-dots conjugated Streptavidin were linked to biotin marked Tau monomers at 4 °C for 10 min, then incubate the SH-SY5Y cells in Opti-MEM culture medium for 4 h, change fresh cell culture medium containing 10 μM Congo red, after 12 h, cells were stained with Annexin V-FITC, observed by laser scanning confocal microscopy (Tokyo, Japan).

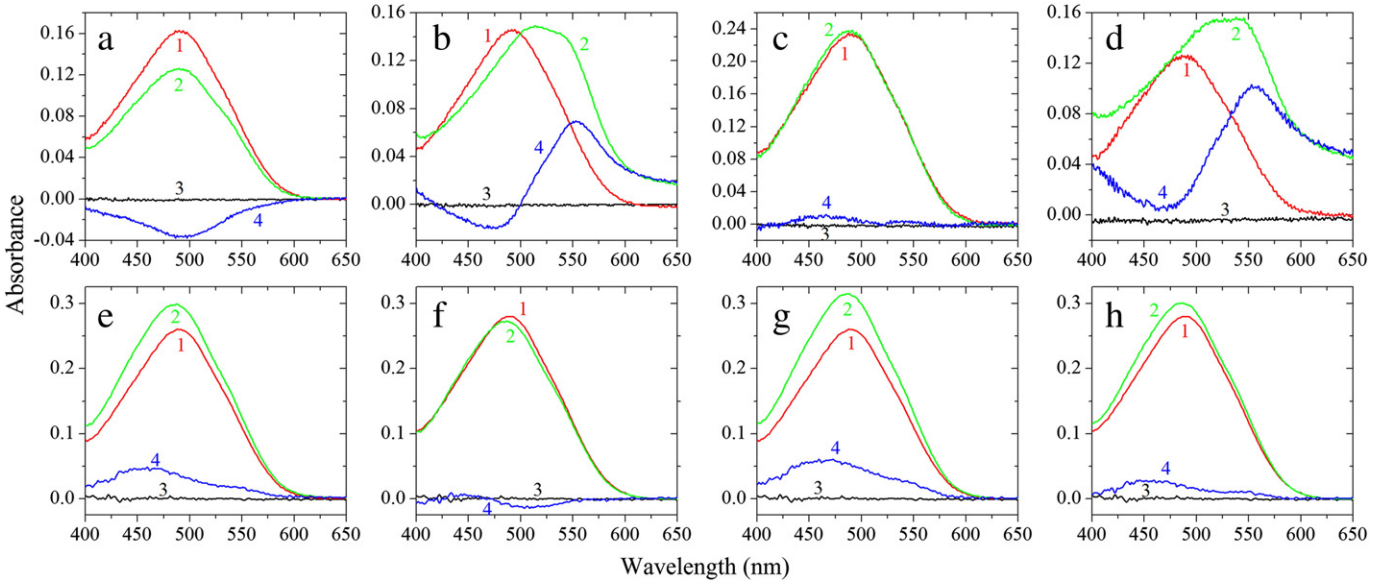


**Fig. 1.** Fibril-forming motifs are essential and sufficient for the fibrillization of human $Tau_{244–372}$ — Congo red binding assays. Absorbance data are shown for amyloid fibril formation of 5 μM wild-type $Tau_{244–372}$ in the presence of 50 μM Congo red at 0 h (a) and 2 h (b), respectively, and that of 5 μM $Tau_{244–372}$/ΔPHF6/ΔPHF6* inserted by IFQINS at the location of PHF6 (positive insertion mutant) in the presence of 50 μM Congo red at 0 h (c) and 12 h (d), respectively. No aggregation was detected when either 5 μM $Tau_{244–372}$/ΔPHF6/ΔPHF6* (double deletion mutant) was incubated with 50 μM Congo red at 0 h (e) and 12 h (f), respectively, or 5 μM $Tau_{244–372}$/ΔPHF6/ΔPHF6* inserted by GGGGGG at the location of PHF6 (negative insertion mutant) was incubated with 50 μM Congo red at 0 h (g) and 12 h (h), respectively. In each panel, the difference spectra (4) were obtained by subtracting the absorbance spectra of Tau alone (3) and Congo red alone (1) from those of Tau + Congo red (2). Congo red binding assays were carried out at 37 °C.

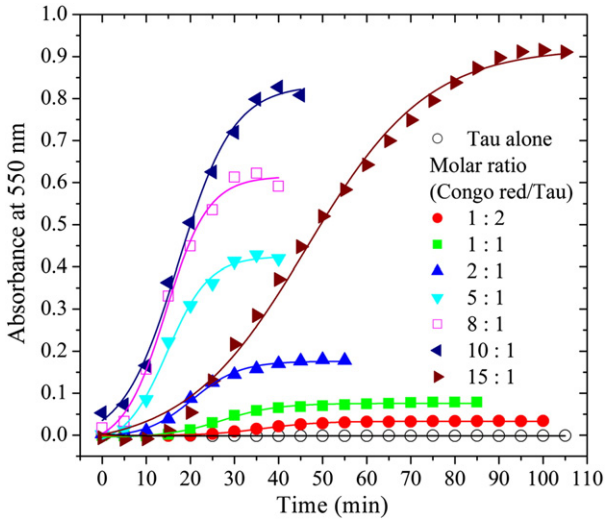


**Fig. 2.** The dependence of changes in the absorbance at 550 nm for $Tau_{244–372}$ filament formation at 37 °C on the molar ratio of Congo red to Tau protein. The concentrations of $Tau_{244–372}$ and DTT were 10 μM and 2 mM, respectively. The molar ratio of Congo red to $Tau_{244–372}$ was 1:2 (filled circle), 1:1 (filled square), 2:1 (filled triangle), 5:1 (inverted filled triangle), 8:1 (open square), 10:1 (left filled triangle), and 15:1 (right filled triangle), respectively. 10 μM $Tau_{244–372}$ alone (open circle) was as control. A sigmoidal equation was fitted to all data from replicates at each Congo red concentration.

**Table 1**
Kinetic parameters of Tau fibrillization in the presence of different concentrations of Congo red as determined by Congo red binding assays at 37 °C. Kinetic parameters, $k$, $t_m$ and the lag time, were determined by fitting the absorbance at 550 nm *versus* time in Figs. 2 and 3 to Eq. (1). The final concentration of $Tau_{244–372}$ was 10 μM. The buffer used was 10 mM HEPES buffer (pH 7.4) containing 2 mM DTT and 100 mM NaCl. Errors shown are standard errors of the mean.

| Tau | Congo red | $k$ | $t_m$ | Lag time |
|---|---|---|---|---|
| | μM | $10^{-3}$ $min^{-1}$ | min | min |
| $Tau_{244–372}$ | 0 | ~0[a] | NA[b] | NA[b] |
| | 5 | 155 ± 14 | 36.5 ± 2.6 | 23.6 ± 3.8 |
| | 10 | 160 ± 15 | 27.2 ± 2.7 | 14.7 ± 3.9 |
| | 20 | 187 ± 19 | 20.5 ± 2.5 | 9.8 ± 3.6 |
| | 50 | 210 ± 29 | 14.8 ± 3.0 | 5.3 ± 4.3 |
| | 80 | 208 ± 31 | 14.4 ± 3.3 | 4.8 ± 4.7 |
| | 100 | 159 ± 19 | 17.2 ± 3.5 | 4.6 ± 5.0 |
| | 150 | 61.1 ± 3.7 | 44.1 ± 4.4 | 11.4 ± 6.4 |
| | 50[c] | 139 ± 2 | 27.3 ± 0.5 | 12.9 ± 0.7 |
| Positive insertion mutant[d] | 50[c] | 11.5 ± 0.7 | 407 ± 2 | 232 ± 13 |
| Double deletion mutant[e] | 50[c] | ~0[a] | NA[b] | NA[b] |
| Negative insertion mutant[f] | 50[c] | ~0[a] | NA[b] | NA[b] |

[a] Observed from the absorbance spectra directly.
[b] No aggregation observed in the present conditions.
[c] The final concentration of Tau protein was 5 μM.
[d] $Tau_{244–372}$/ΔPHF6/ΔPHF6* inserted by IFQINS at the location of PHF6.
[e] $Tau_{244–372}$/ΔPHF6/ΔPHF6*.
[f] $Tau_{244–372}$/ΔPHF6/ΔPHF6* inserted by GGGGGG at the location of PHF6.

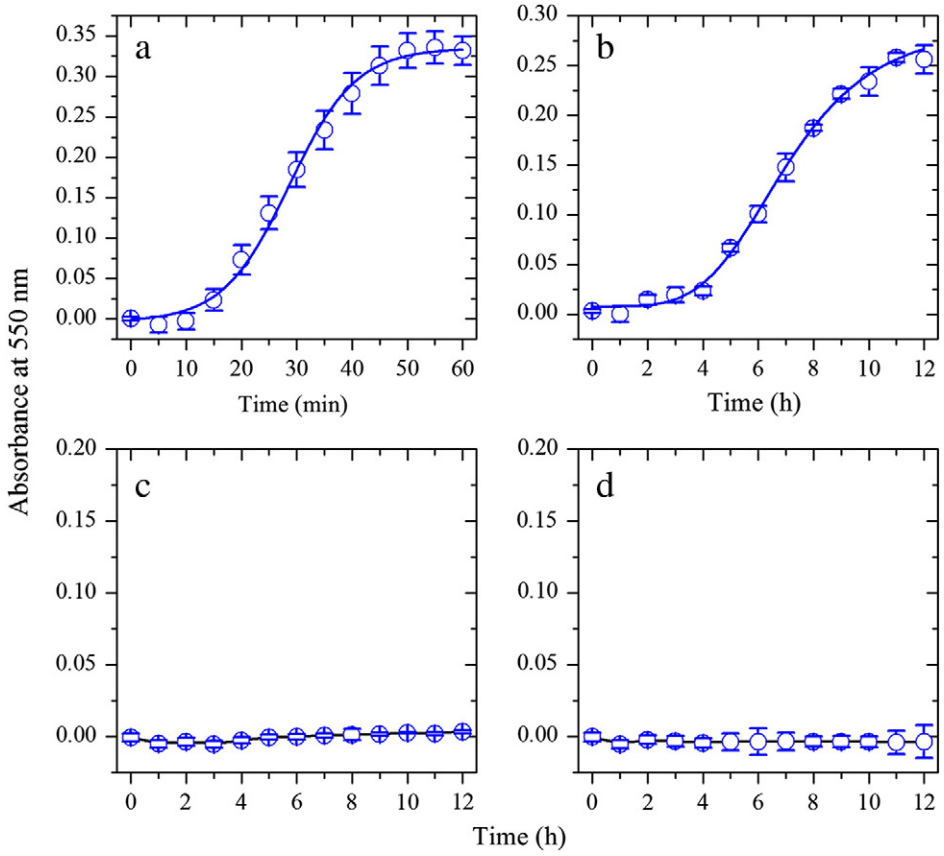


**Fig. 3.** Fibril-forming motifs are essential and sufficient for the fibrillization of human $Tau_{244–372}$— kinetic analyses based on absorbance data at 550 nm. Kinetic curves for the aggregation of 5 μM wild-type $Tau_{244–372}$ (a) and 5 μM $Tau_{244–372}$/ΔPHF6/ΔPHF6* inserted by IFQINS at the location of PHF6 (b), incubated with 50 μM Congo red. A sigmoidal equation was fitted to all data (open circles). No aggregation was detected when either 5 μM $Tau_{244–372}$/ΔPHF6/ΔPHF6* was incubated with 50 μM Congo red up to 12 h (c) or 5 μM $Tau_{244–372}$/ΔPHF6/ΔPHF6* inserted by GGGGGG at the location of PHF6 was incubated with 50 μM Congo red up to 12 h (d). Absorbance data with error bars were expressed as mean ± S.D. of 3 independent experiments. Congo red binding assays were carried out at 37 °C.

### 2.11. Annexin V-FITC apoptosis detection assay

Apoptotic cells were detected by flow cytometry after staining with Annexin V-FITC apoptosis detection kit (Beyotime, Nantong, China). Briefly, cells treated with Tau monomers were collected, washed with PBS buffer and re-suspended in 195 μl of binding buffer containing 5 μl annexin V-FITC, after 10 min of incubation in darkness at room temperature, centrifugated at 1000 *g* for 5 min and re-suspended in 190 μl of binding buffer containing 10 μl propidium iodide (PI). Annexin V binding was analyzed by an EPICS XL-MCL flow cytometer (Beckman Coulter, Fullerton, CA). The percentage of apoptotic cells was calculated from the total (~$10^4$ cells) using EXPO32 MultiComp software (Beckman Coulter). Viable cells did not bind annexin V or PI (lower left quadrant D3), early apoptotic cells bound to annexin V but excluded PI (lower right quadrant D4), and necrotic or late apoptotic cells were both annexin V- and PI-positive (upper right quadrant D2). The upper left quadrant D1 contains the cells damaged during the preparation of the cell suspension.

## 3. Results

### 3.1. Effect of Congo red on fibril formation of human Tau protein in vitro

In this study, the effects of Congo red on filament formation of human Tau fragment $Tau_{244–372}$ were examined by Congo red binding assays (Figs. 1–3 and S1). The following are the reasons why Congo red was used from biological and pathological viewpoints. Firstly, Congo red is a small molecule that acts as an inducer of Tau aggregation, and the kinetic barrier to Tau fibrillization can be overcome by Congo red [25]. Secondly, Congo red is a well-known histological stain for demonstrating the presence of amyloidosis in fixed tissues by reacting specifically with β-sheet-rich amyloid fibrils stoichiometrically, and the bound form displays a characteristic red shift in its maximum absorbance from 490 to 550 nm [33,34]. Based on absorbance at 550 nm which is representing the amounts of Tau fibrils, we can quantitatively characterize Tau fibrillization induced by Congo red. Thirdly, Congo red is able to cross the membrane and has thus been employed as an agonist into an inducible cell model for some amyloidogenic proteins

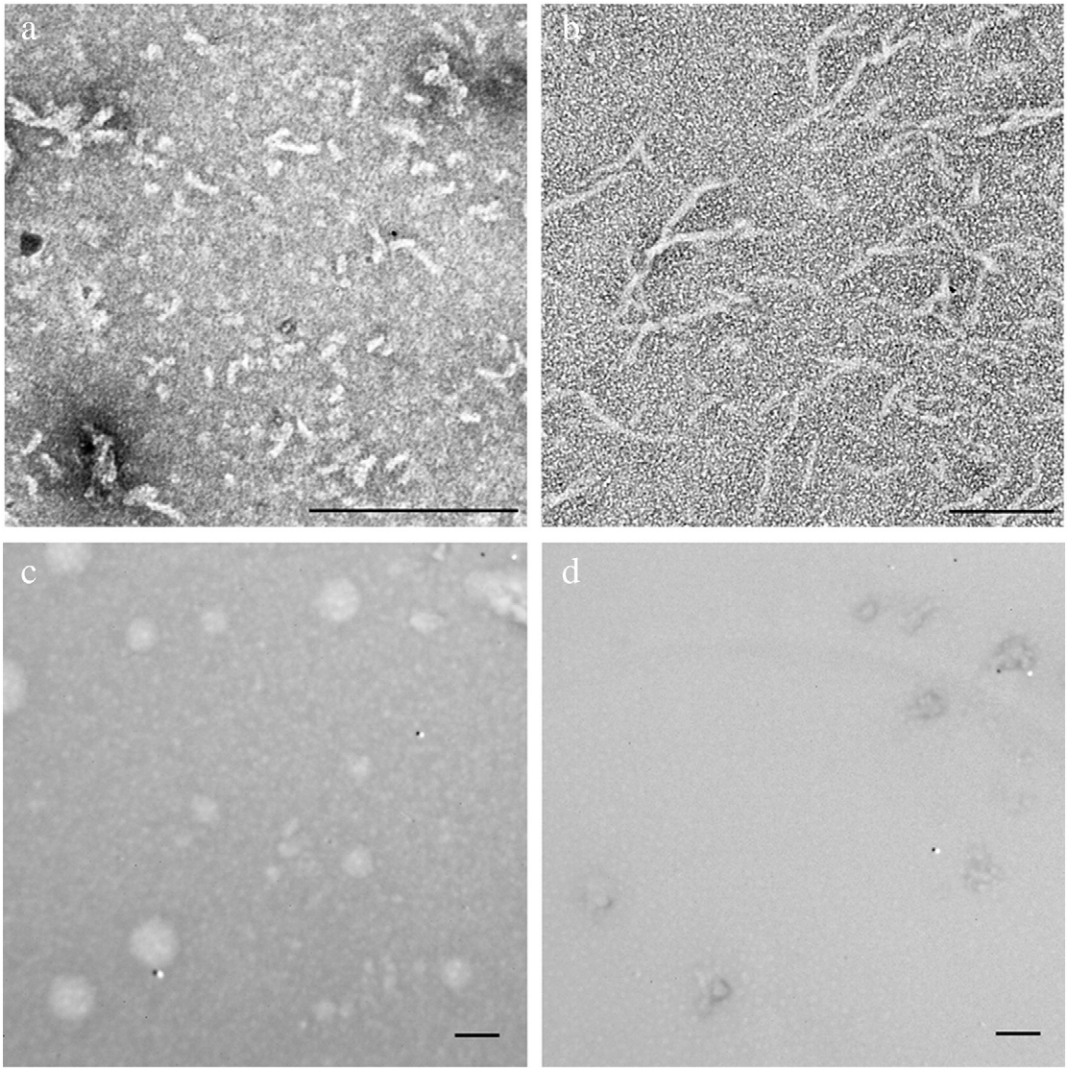


**Fig. 4.** Fibril-forming motifs are essential and sufficient for the fibrillization of human $Tau_{244–372}$— TEM measurements. Negative-stain transmission electron micrographs of 5 μM wild-type $Tau_{244–372}$ (a), 5 μM $Tau_{244–372}$/ΔPHF6/ΔPHF6* inserted by IFQINS at the location of PHF6 (b), 5 μM $Tau_{244–372}$/ΔPHF6/ΔPHF6* (c), and 5 μM $Tau_{244–372}$/ΔPHF6/ΔPHF6* inserted by GGGG GG at the location of PHF6 (d), incubated with 50 μM Congo red at 37 °C for 45 min (a) or 12 h (b, c, and d). Amyloid fibrils were clearly observed in a and b. In contrast, no aggregates were observed in c and d. All the scale bars were 200 nm.

[26]. Fig. 1a and b shows amyloid fibril formation of wild-type $Tau_{244–372}$ induced by Congo red at 0 and 2 h, respectively, and Fig. 1c and d shows that of $Tau_{244–372}$/ΔPHF6/ΔPHF6* inserted by IFQINS at the location of PHF6 (positive insertion mutant) induced by Congo red at 0 and 12 h, respectively. Fig. S1A and B displays amyloid fibril formation of $Tau_{244–372}$/ΔPHF6 induced by Congo red at 0 and 12 h, respectively, and Fig. S1C and D displays that of $Tau_{244–372}$/ΔPHF6* induced by Congo red at 0 and 12 h, respectively. As shown in Figs. 1 and S1, the absorbance of Tau was almost unobservable between 400 and 650 nm, and Congo red had a characteristic absorbance peak at around 490 nm. A red shift of the maximum absorbance of Congo red from 490 nm to 550 nm occurred for wild-type $Tau_{244–372}$, its positive insertion mutant, PHF6-deleted mutant, and PHF6*-deleted mutant in the presence of 50 μM Congo red (Fig. 1b and d, and Fig. S1B and D), which is one of the characteristic features of amyloid fibrils [33,34]. In contrast, in the presence of 50 μM Congo red, no red shift of the maximum absorbance of this dye was observed for either $Tau_{244–372}$/ΔPHF6/ΔPHF6* (double deletion mutant) or $Tau_{244–372}$/ΔPHF6/ΔPHF6* inserted by GGGGGG at the location of PHF6 (negative insertion mutant), and the absorbance spectrum of Tau + Congo red was almost the same as that of Congo red alone (Fig. 1f and h), indicating that no aggregation was detected when either the double deletion mutant or the negative insertion mutant was incubated with this inducer up to 12 h. Our Congo red binding data indicate that fibril-forming motifs are essential and sufficient for the fibrillization of human $Tau_{244–372}$ induced by Congo red *in vitro*.

Aggregation kinetics can be achieved by detecting the absorbance at 550 nm continuously (Figs. 2 and 3). We then used a sigmoidal equation [8,9,31,32] to fit the kinetic data, in order to elucidate the detailed effects of Congo red on amyloid fibril formation of wild-type

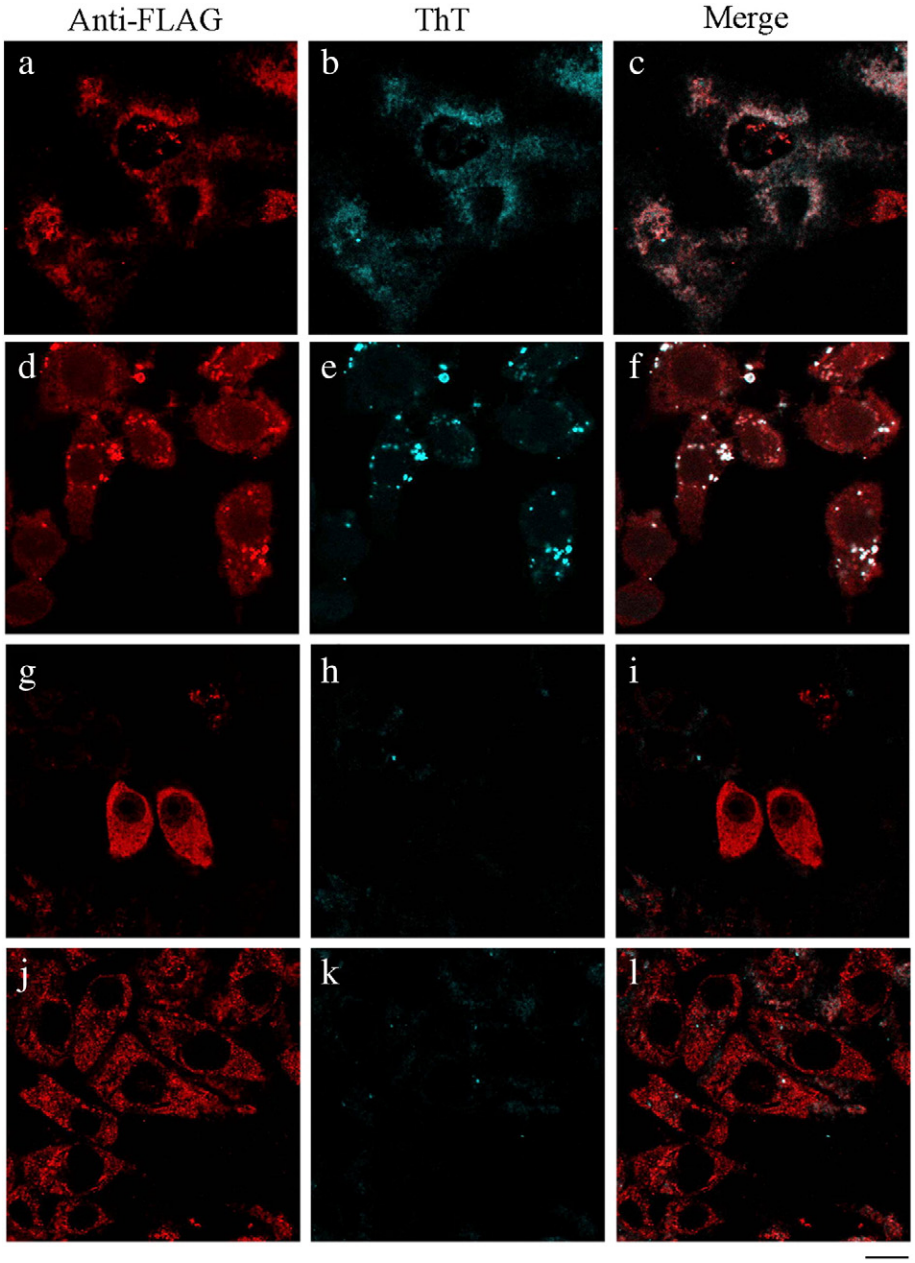


**Fig. 5.** Sequence-dependent abnormal aggregation of human $Tau_{244–372}$ in SH-SY5Y cells. Wild-type $Tau_{244–372}$ (a–c) and $Tau_{244–372}$/ΔPHF6/ΔPHF6* inserted by IFQINS at the location of PHF6 (d–f) over-expressed in SH-SY5Y neuroblastoma cells formed aggregates in the cells. In contrast, no aggregates were observed in either $Tau_{244–372}$/ΔPHF6/ΔPHF6* over-expressed SH-SY5Y cells (g–i) or $Tau_{244–372}$/ΔPHF6/ΔPHF6* inserted by GGGGGG at the location of PHF6 over-expressed SH-SY5Y cells (j–l). SH-SY5Y cells were stained with 250 μM ThT, coimmunostained with primary monoclonal antibodies anti-FLAG and secondary Alexa Fluo-546, and visualized by confocal microscopy. The scale bar represents 10 μm.

$Tau_{244–372}$ and its mutants. Three kinetic parameters, $k$, $t_m$, and the lag time, were determined by fitting the absorbance at 550 nm *versus* time to this equation, and the best fit to each data set, calculated using the parameter values given in Table 1, was plotted together with the data in Figs. 2 and 3. As shown in Table 1, the optimal molar ratio of Congo red to wild-type $Tau_{244–372}$ is 10:1 for the shortest lag time, which is similar to the optimal molar ratio of Congo red to full-length human Tau as previously reported [25,26].

To get a better understanding about the effect of Congo red on Tau aggregation, we performed kinetic analyses based on the absorbance at 550 nm using the optimal molar ratio of Congo red to Tau of 10:1. As is shown in Fig. 3 and Table 1, aggregation was observed for both wild-type $Tau_{244–372}$ and its positive insertion mutant in the presence of 50 μM Congo red (Fig. 3a and b). In contrast, no aggregation was detected when either the double deletion mutant or the negative insertion mutant was incubated with 50 μM Congo red up to 12 h (Fig. 3c and d). The above data once again demonstrate that fibril-forming motifs are essential and sufficient for the fibrillization of human $Tau_{244–372}$ induced by Congo red *in vitro*.

To further prove Congo red induced Tau aggregation *in vitro*, TEM was employed to study the morphology of Tau incubated with Congo red. Amyloid fibrils were clearly observed in negative-stain transmission electron micrographs of both wild-type $Tau_{244–372}$ and its positive insertion mutant in the presence of 50 μM Congo red (Fig. 4a and b). As shown in Fig. 3a and b and Fig. 4a and b, fibrils formed from wild-type $Tau_{244–372}$ and its positive insertion mutant were of different kinetic parameters and different morphologies. Wild-type $Tau_{244–372}$ produced abundant short amyloid fibrils at 45 min (Fig. 4a) and abundant long and branched fibrils at 12 h (data not shown) with shorter lag time (Fig. 3a), but the positive insertion mutant produced some short filaments and many fibrils with a length of 100–200 nm at 12 h (Fig. 4b) with much longer lag time (Fig. 3b). By contrast, no aggregates were observed when either the double deletion mutant or the negative insertion mutant was incubated with Congo red up to 12 h (Fig. 4c and d). We could address such distinct kinetics and morphologies in light of sequence-dependent abnormal aggregation of Tau. However, the possibility that changes in structures and/or solubility of Tau result in such distinct kinetics and morphologies cannot be excluded.

We concluded from the results of TEM and Congo red binding assay that human Tau aggregation induced by Congo red is sequence-dependent *in vitro*. When its two fibril-forming segments PHF6 and PHF6* were deleted, human Tau fragment $Tau_{244–372}$ did lose its ability to form fibrils induced by Congo red, and the insertion of an unrelated amyloid core sequence IFQINS from human lysozyme into the disabled Tau protein did retrieve its ability to form fibrils. By contrast, insertion of a non-fibril forming peptide GGGGGG did not drive the disabled Tau protein to misfold *in vitro*.

### *3.2. Fibril-forming motifs are essential and sufficient for Tau fibrillization in SH-SY5Y cells*

Here, we first established an inducible cell model which used Congo red as the agonist to examine whether the aggregation of human Tau in SH-SY5Y neuroblastoma cells is sequence-dependent or not. SH-SY5Y cells transiently over-expressing FLAG-tagged wild-type $Tau_{244–372}$, the positive insertion mutant, PHF6-deleted mutant, PHF6*-deleted mutant, the double deletion mutant, and the negative insertion mutant were incubated with 10 μM Congo red for 3 days, planted onto the coverslips in the presence of 10 μM Congo red for 3 days, and then transfected with plasmids transiently (Figs. 5 and S2). As shown in Figs. 5 and S2, wild-type $Tau_{244–372}$ (a–c), its positive insertion mutant (d–f), PHF6-deleted mutant (a–c), and PHF6*-deleted mutant (d–f) over-expressed in SH-SY5Y cells formed aggregates in the cells, as detected by immunofluorescence using anti-FLAG antibody (red) and ThT staining (green), an amyloid-binding dye, and the merge image (light gray or white) demonstrated co-localization of transiently over-expressed wild-type $Tau_{244–372}$ or its positive insertion mutant or its single deletion mutants with ThT-positive amyloids. In contrast, no aggregates were observed in either the double deletion mutant (Fig. 5g–i) or the negative insertion mutant (Fig. 5j–l) over-expressed SH-SY5Y cells, since co-localization of immunofluorescence and ThT staining was invisible as detected by immunofluorescence using anti-FLAG antibody (red) and ThT staining (green invisible). Therefore, we first demonstrated sequence-dependent abnormal aggregation of human Tau in SH-SY5Y cells induced by Congo red.

Because the cells were exposed to 10 μM Congo red for extended periods of time, and might react differently from naive cells, we did the following control experiment with pathogenic mutations that favor Tau aggregation in the absence of Congo red (Fig. S3). As shown in Fig. S3b and c, some of the ThS stain is outside of cells expressing $Tau_{244–372}$ΔK280, as indicated by anti-FLAG immunostaining. As shown in Fig. S3, both $Tau_{244–372}$ΔK280 stably expressed in SH-SY5Y cells (a–d) and endogenous human Tau (e–h) formed aggregates in the cells even in the absence of Congo red, as detected by immunofluorescence using anti-FLAG antibody (red) or TAU-5 (red) and ThS staining (green), another amyloid-binding dye, and the merge image (white) demonstrated co-localization of both stably expressed $Tau_{244–372}$ΔK280 and endogenous human Tau with ThS-positive amyloids. Clearly, ThS staining is detecting both endogenous human Tau aggregates and $Tau_{244–372}$ΔK280 aggregates in Fig. S3b and c. Therefore, abnormal aggregation of human Tau in SH-SY5Y cells is sequence-dependent but not Congo red-dependent.

Then, we applied Western blot to confirm Congo red induced Tau aggregation in Tau over-expressed SH-SY5Y cells. SH-SY5Y cell lysis was separated into supernatant and pellet fractions by ultracentrifugation. Western blot bands in a and b of cell lysate were present to confirm that wild-type $Tau_{244–372}$ and its mutants did over-express in SH-SY5Y cells (Figs. 6 and S4). Wild-type $Tau_{244–372}$, its positive insertion mutant, PHF6-deleted mutant, and PHF6*-deleted mutant over-expressed in SH-SY5Y cells formed aggregates in the cells, as observed in the pellet fraction (Fig. 6a and b and Fig. S4a and b). By contrast, no aggregates were observed in either the double deletion mutant or the negative insertion mutant over-expressed SH-SY5Y cells, since the pellet fraction was invisible (Fig. 6c and d).

To further confirm sequence-dependent fibril formation of human Tau in SH-SY5Y cells, immunogold electron microscopy was applied to survey the morphology of Tau aggregates extracted from Congo red-treated, Tau over-expressed SH-SY5Y cells and visualized by immunoelectron microscopy using monoclonal anti-FLAG primary antibody and 10-nm gold-labeled secondary antibody. Aggregates extracted from wild-type $Tau_{244–372}$ and its positive insertion mutant over-expressed SH-SY5Y cells were labeled by gold particles, and fibrils highlighted by using red arrowheads were observed in both cases (Fig. 7a and b). We conclude that such filaments are composed of Tau protein from these stains. In contrast, no aggregates were observed in

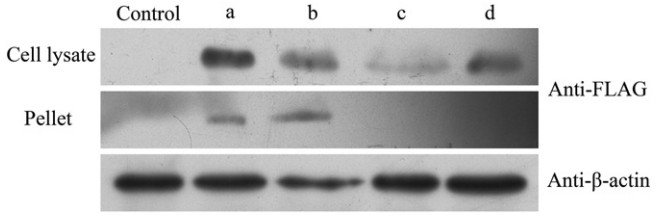


**Fig. 6.** Fibril-forming motifs are essential and sufficient for abnormal aggregation of human $Tau_{244–372}$ in SH-SY5Y cells — Western blot. Wild-type $Tau_{244–372}$ (a) and $Tau_{244–372}$/ΔPHF6/ΔPHF6* inserted by IFQINS at the location of PHF6 (b) over-expressed in SH-SY5Y neuroblastoma cells formed aggregates in the cells. In contrast, no aggregates were observed in either $Tau_{244–372}$/ΔPHF6/ΔPHF6* expressed SH-SY5Y cells (c) or $Tau_{244–372}$/ΔPHF6/ΔPHF6* inserted by GGGGGG at the location of PHF6 over-expressed SH-SY5Y cells (d). Immunoreactive bands were visualized by enhanced chemiluminescence. Immunoblots for cell lysates, and ultracentrifugation pellets, and β-actin were shown.

either the double deletion mutant or the negative insertion mutant over-expressed SH-SY5Y cells (Fig. 7c and d).

Combining the results from immunofluorescence, Western blot, and immunogold electron microscopy, we conclude that fibril-forming motifs are essential and sufficient for abnormal aggregation of human Tau in SH-SY5Y cells induced by Congo red: when its two fibril-forming segments PHF6 and PHF6* are deleted, human Tau fragment $Tau_{244–372}$ did lose its ability to form fibrils in SH-SY5Y cells, and the replacement of PHF6 and PHF6* with an unrelated amyloidogenic sequence IFQINS from human lysozyme did rescue the fibril-forming ability of $Tau_{244–372}$ in SH-SY5Y cells. These fibril-forming motifs themselves (PHF6, PHF6*, and IFQINS) can form amyloid fibrils *in vitro* and in cells [13,14]. We demonstrate for the first time that insertion of such a fibril-forming motif can replace PHF6/PHF6* motifs, forcing human Tau to form fibrils in cells. By contrast, insertion of a non-fibril forming peptide GGGGGG did not drive the disabled $Tau_{244–372}$ to misfold in SH-SY5Y cells.

### *3.3. Fibril-forming motifs are essential and sufficient for early apoptosis of living SH-SY5Y cells induced by abnormal aggregation of human Tau*

As mentioned above, $Tau_{244–372}$ formed amyloid fibrils induced by Congo red both *in vitro* and in SH-SY5Y cells, we want to know whether such abnormal aggregation can induce early apoptosis of SH-SY5Y cells. In the early stages of apoptosis, the cell membrane can expose phosphatidylserine which is annexin V-positive [35]. We then apply Q-dots based probes combined with annexin V staining to detect early apoptosis of living SH-SY5Y cells induced by abnormal aggregation of

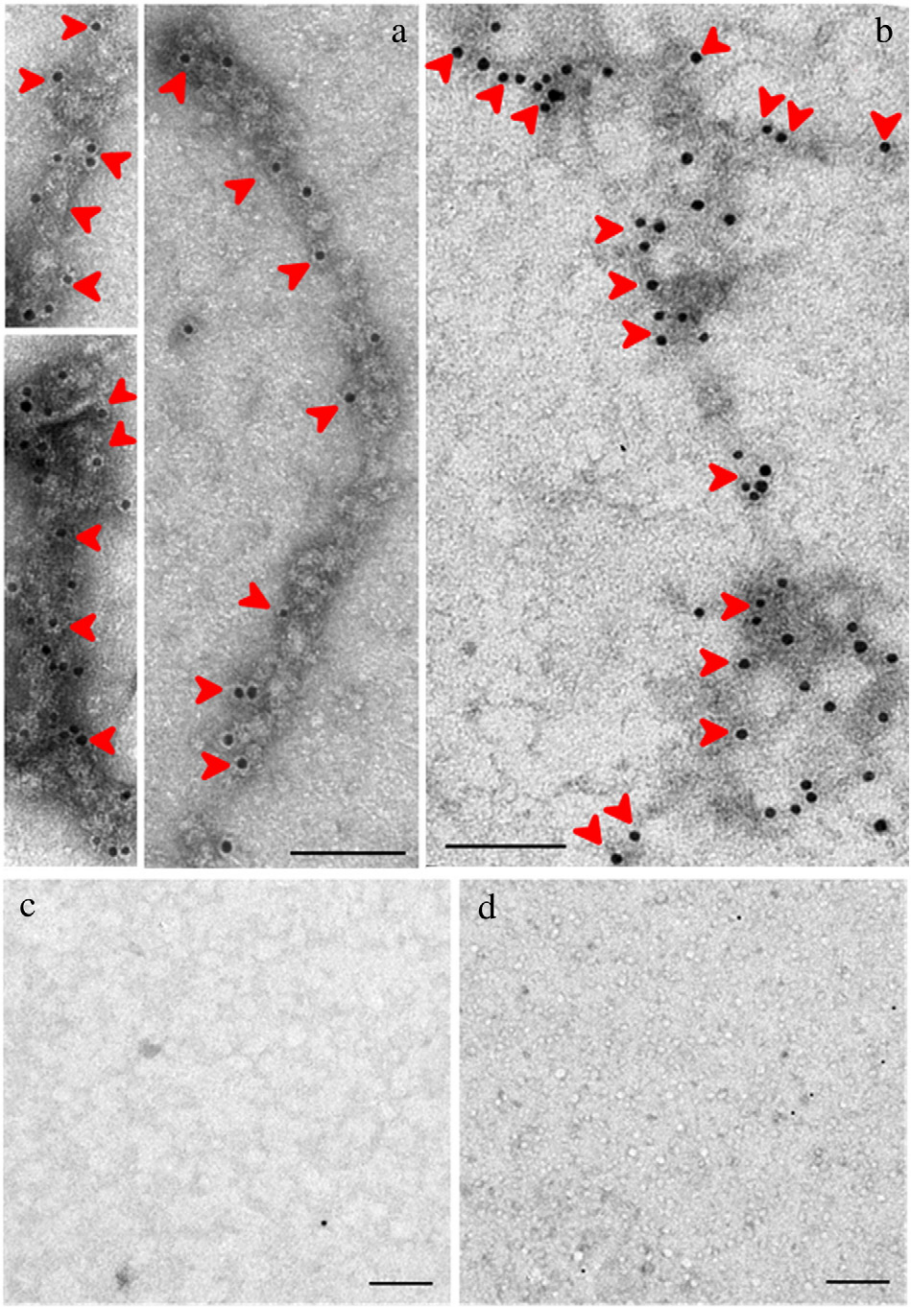


**Fig. 7.** Fibril-forming motifs are essential and sufficient for the fibrillization of human $Tau_{244–372}$ in SH-SY5Y cells — immunogold electron microscopy. Aggregates extracted from wild-type $Tau_{244–372}$ (a) and $Tau_{244–372}$/ΔPHF6/ΔPHF6* inserted by IFQINS at the location of PHF6 (b) were labeled by gold particles, and fibrils, highlighted by using red arrowheads, were observed in both cases (a and b). In contrast, no aggregates were observed in either $Tau_{244–372}$/ΔPHF6/ΔPHF6* over-expressed SH-SY5Y cells (c) or $Tau_{244–372}$/ΔPHF6/ΔPHF6* inserted by GGGGGG at the location of PHF6 over-expressed SH-SY5Y cells (d). The scale bars represent 100 nm.

human Tau. As shown in Fig S5, Q-dots labeled wild-type $Tau_{244–372}$ monomers can be transported into living SH-SY5Y cells conveniently. Apoptotic cells were stained with an Annexin V-conjugated organic dye FITC. As shown in Fig. 8, wild-type $Tau_{244–372}$ monomer, the positive insertion mutant monomer, the double deletion mutant monomer, and the negative insertion mutant monomer, all labeled by Q-dots (red), entered into living SH-SY5Y cells through endocytosis, and mainly located in the cytoplasm. Wild-type $Tau_{244–372}$ monomer (Fig. 8a–d) and its positive insertion mutant monomer (Fig. 8e–h) marked by Q-dots formed aggregates and thus induced early apoptosis of living SH-SY5Y cells, as marked by Annexin V-FITC (green) binding to phosphatidylserine moieties on the outer membrane of the cells (Fig. 8b, c, f, and g). In contrast, such early apoptosis of living SH-SY5Y cells was not observed in either the double deletion mutant monomer (Fig. 8i–l) or the negative insertion mutant monomer (Fig. 8m–p) marked by Q-dots (Fig. 8j, k, n, and o). Furthermore, no early apoptosis was observed either in living SH-SY5Y cells cultured in Congo red alone (Fig. S6a) or in living SH-SY5Y cells cultured in Congo red incubated with Q-dots (Fig. S6b), indicating that either Congo red itself or Q-dots themselves cannot induce apoptosis of SH-SY5Y cells.

The difference between apoptosis and cell necrosis is that during the early stages of apoptosis the cell membrane remains intact, while during necrosis the cell membrane loses its integrity and becomes leaky [36]. Therefore the measurement of annexin V binding to the cell surface as indicative for apoptosis should be performed in combination with the membrane-impermeable DNA stain PI to distinguish three different cell types during apoptosis: viable cells (annexin V- and PI-negative), early apoptotic cells (annexin V-positive but PI-negative),

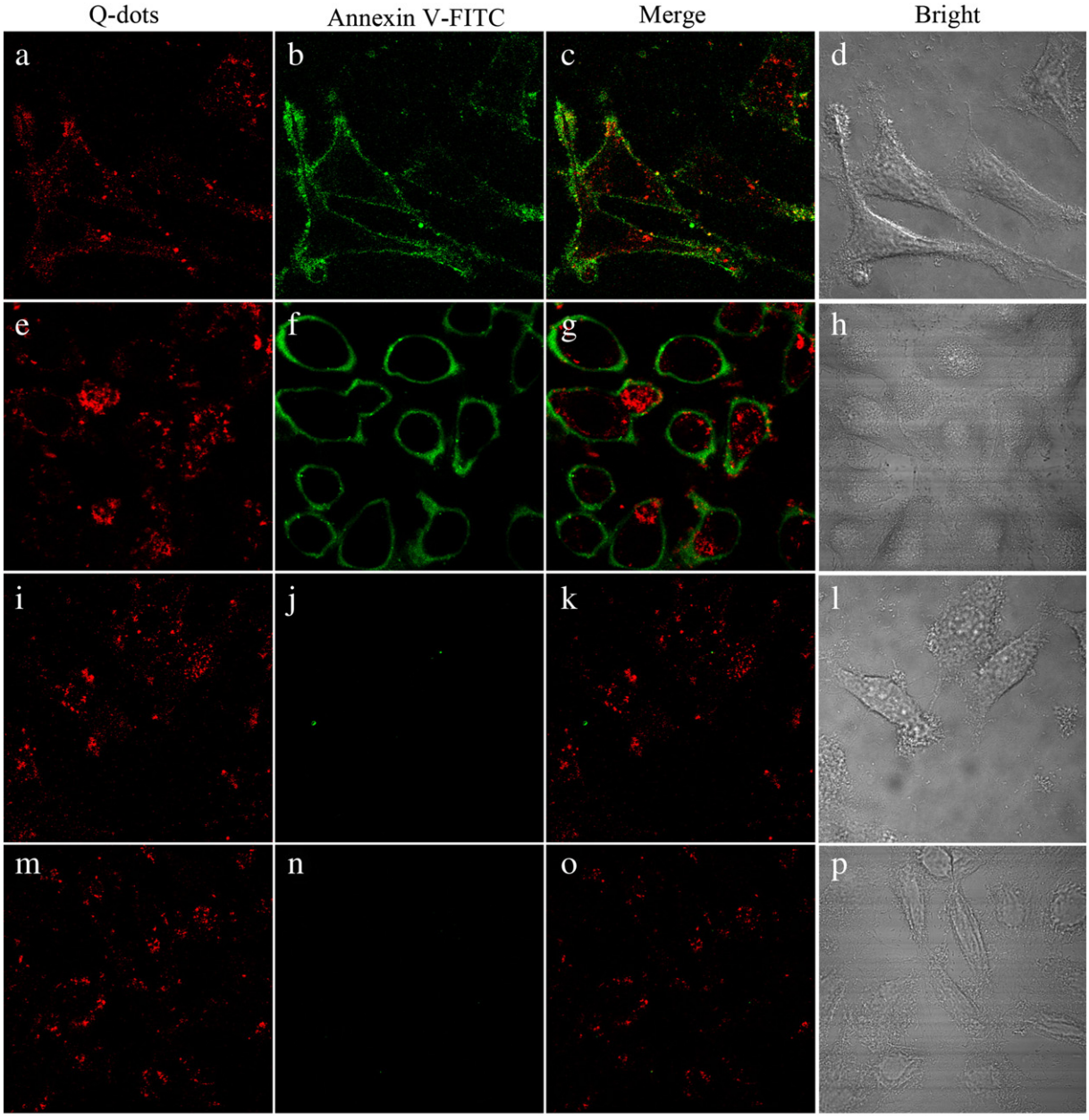


**Fig. 8.** Fibril-forming motifs are essential and sufficient for early apoptosis of living SH-SY5Y cells induced by abnormal aggregation of human $Tau_{244–372}$— quantum dots based probes combined with annexin V staining. Wild-type $Tau_{244–372}$ monomer (a–d) and $Tau_{244–372}$/ΔPHF6/ΔPHF6* monomer inserted by IFQINS at the location of PHF6 (e–h) marked by quantum dots formed aggregates and thus induced early apoptosis of living SH-SY5Y neuroblastoma cells. In contrast, early apoptosis of SH-SY5Y cells was not observed in either $Tau_{244–372}$/ΔPHF6/ΔPHF6* (i–l) or $Tau_{244–372}$/ΔPHF6/ΔPHF6* inserted by GGGGGG at the location of PHF6 marked by quantum dots (m–p). Living SH-SY5Y cells were stained with Annexin V-FITC, and observed by confocal laser scanning microscopy. The scale bar represents 10 μm.

and necrotic or late apoptotic cells (annexin V- and PI-positive) [36]. Here, we performed double-staining using annexin V-FITC and PI followed by flow cytometry. As shown in Fig. 9, the percentage of early apoptotic cells in Congo red cultured living SH-SY5Y cells incubated with wild-type $Tau_{244–372}$ monomer (a) and its positive insertion mutant monomer (b) for 12 h was 19.50% and 11.48% respectively, much higher than that of the double deletion mutant (c, 3.90%) and the negative insertion mutant (d, 3.08%), while only a very small amount of Congo red cultured living SH-SY5Y cells incubated with wild-type $Tau_{244–372}$ and its three mutants for 12 h was late apoptotic or necrotic. In order to distinguish between Tau fragment toxicity and toxicity that occur only in the presence of Congo red, we did the following control experiments and performed statistical analyses by using the Student's *t*-test (Fig S7). As shown in Fig. S7, Congo red itself had no toxicity and even nutritious to SH-SY5Y cells. Our control experiments demonstrated that Congo red treatment is actually nutritious to the cells (Fig. S7).

Combining the results from quantum dots based probes combined with annexin V staining and annexin V-FITC apoptosis detection assay, we conclude that fibril-forming motifs are essential and sufficient for early apoptosis of living SH-SY5Y cells induced by abnormal aggregation of human Tau. We demonstrate for the first time that insertion of a fibril-forming motif IFQINS can replace PHF6/PHF6* motifs, forcing human Tau to form fibrils in living cells and inducing early apoptosis of living cells.

## 4. Discussion

Amyloidogenic proteins, including human Tau [3,7,11,12], amyloid β [37], human α-synuclein [38], and human copper, zinc superoxide dismutase [39], have been investigated *in vivo* to a certain degree. Amyloidogenic proteins studied *in vivo* could be much more significant for the treatment of neurodegenerative diseases. Investigations on human Tau in cells generally focus on its aggregation, which are successful by using agonist inducers [26,27], fibril seeds [40,41], and its pathological mutant-ΔK280 [42–44] to promote its fibrillization. In this study, we employed a Congo red inducible cell model to investigate abnormal aggregation of human Tau in SH-SY5Y cells. We found that fibril-forming motifs are essential and sufficient not only for the fibrillization of human Tau in SH-SY5Y cells, but also for early apoptosis of living SH-SY5Y cells induced by abnormal aggregation of human Tau. Our results suggest that fibril-forming motifs could be the determinants

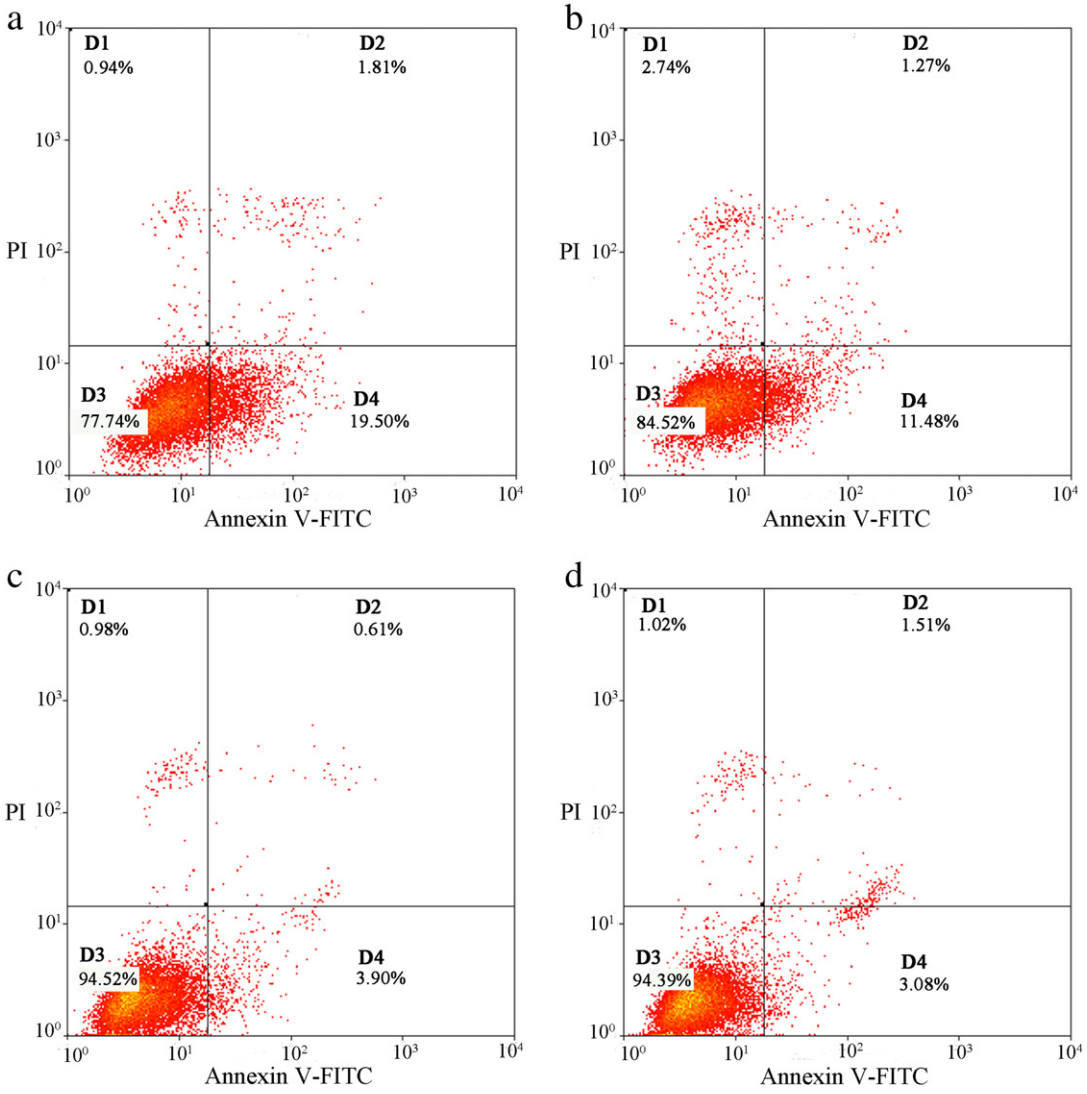


**Fig. 9.** Flow cytometric analysis of annexin V and PI staining shows induction of apoptosis. Congo red cultured living SH-SY5Y cells incubated with wild-type $Tau_{244–372}$ monomer (a) or $Tau_{244–372}$/ΔPHF6/ΔPHF6* monomer inserted by IFQINS (b) for 12 h showed much higher rate of early apoptosis than that of $Tau_{244–372}$/ΔPHF6/ΔPHF6* monomer (c) or $Tau_{244–372}$/ΔPHF6/ΔPHF6* monomer inserted by GGGGGG (d) for 12 h. The percentage of apoptotic cells was detected by analyzing annexin V-FITC and PI binding with the help of the Submit 3.0 software. Viable cells did not bind annexin V or PI (lower left quadrant D3), early apoptotic cells bound to annexin V but excluded PI (lower right quadrant D4), and necrotic or late apoptotic cells were both annexin V- and PI-positive (upper right quadrant D2). The upper left quadrant D1 contains the cells damaged during the preparation of the cell suspension.

of human Tau protein tending to misfold in living cells, thereby inducing neuronal apoptosis and causing the initiation and development of tauopathies. The data of positive and negative control mutants with double deletion mutants increased reliability of our suggestion.

Congo red, being a commonly used histological dye for amyloid detection, possesses the capacity to interfere with processes of protein misfolding and aggregation [45]. Its absorbance peak displays a red shift in UV–visible absorbance spectrum after binding fibrils and it is a diagnostic stain presenting characteristic apple-green birefringence [27,33,34,46]. Congo red has been found to bind to the prion-forming domain of HET-s prion with a ten-fold molar excess of Congo red [47]. Heteronuclear NMR data also show that Congo red at lower concentrations mainly interacts with the N-terminal and central regions of α-synuclein, binding to monomeric α-synuclein and promoting fibrillization [48]. Congo red at lower concentrations also populates partially unfolded states of an amyloidogenic protein to enhance amyloid fibril formation [49]. However, Congo red at higher concentrations stabilizes amyloid β monomer, inhibits its oligomerization, and reduces β-amyloid neurotoxicity [50]. Congo red at higher concentrations also blocks the structural conversion of normal prion protein into its aggregation-competent pathogenic form [51,52]. The kinetic barrier to Tau fibrillization can be overcome by Congo red [25]. Considering its transmembrane ability, Congo red has been employed as an agonist into an inducible cell model for some amyloidogenic proteins [26]. We firstly studied the effect of Congo red on fibril formation of human Tau fragments *in vitro*, and found that human Tau aggregation induced by Congo red is sequence-dependent *in vitro*. When its two fibril-forming segments PHF6 and PHF6* were deleted, human $Tau_{244–372}$ did lose its ability to form fibrils induced by Congo red, and the insertion of an unrelated amyloid core sequence into the disabled $Tau_{244–372}$ did retrieve its ability to form fibrils. By contrast, insertion of a non-fibril forming peptide did not drive the disabled $Tau_{244–372}$ to misfold *in vitro*. Very recently, it has been demonstrated that deletion of PHF6 and PHF6* does abolish the seeding activity of recombinant full-length Tau, suggesting that its aggregation is necessary for seeding [53]. We then investigated sequence-dependent abnormal aggregation of human $Tau_{244–372}$ in an inducible cell model by using Congo red as an agonist, and found that that PHF6 and PHF6* facilitated fibril formation of $Tau_{244–372}$ in SH-SY5Y cells cultured in the presence of Congo red. We also found that an exogenous fibril-forming motif from human lysozyme was able to facilitate fibril formation of this Tau fragment in this cell system. In other words, insertion of other fibril-forming motifs can replace the corresponding motifs of Tau fragment, forcing Tau fragment to form fibrils in cells. A higher percentage of SH-SY5Y cells expressing fibril-forming sequences displayed early stages of apoptosis accompanied by a potential phosphorylation of endogenous human Tau in SH-SY5Y cells that have internalized fibril-forming $Tau_{244–372}$, while non-fibril forming polypeptides had no effect.

Fibril formation of human Tau protein is associated with AD. This paper investigated structural requirements for Tau aggregation inside cultured cells. We focus on the PHF6 and PHF6* motifs previously identified as being essential on the basis of *in vitro* experimentation [19–21]. In our previously published work [19], we showed that the PHF6/PHF6* motifs could be replaced by exogenous amyloidogenic hexapeptide motifs when analyzed in the presence of heparin aggregation inducer. The present study firstly investigated sequence-dependent filament formation of human Tau in cells, inducing early apoptosis of living cells. In the current work, we confirmed the need for at least one amyloidogenic motif in Tau to support aggregation of $Tau_{244–372}$*in vitro* using Congo red as aggregation inducer (a membrane-permeable inducer). We also found that a single amyloidogenic hexapeptide motif at the PHF6 site was necessary and sufficient to support Tau aggregation and toxicity (in the form of apoptosis) in SH-SY5Y cellular environment. Therefore, this paper provides evidence for the conclusion that fibril-forming motifs are essential and sufficient for Tau fibrillization in living cells, much more strongly than our previous study [19]. Clearly, Tau aggregation and toxicity depended on sequences of Tau. However, more than sequence, changes in structures and/or solubility would be alternative explanations. From a macroscopic viewpoint, formation of amyloid fibrils and amorphous aggregates never happens otherwise concentrations of monomers exceed their solubility. Alternatively, changing to amyloidogenic structures (populating amyloidogenic structures) by mutation could be a microscopic explanation.

Based on our own data, we propose a valuable hypothetical model to explain why fibril-forming motifs are so important for driving human Tau to form fibrils in cells (Fig. 10). In the presence of Congo red, wild-type human Tau monomer and its positive insertion mutant monomer, both with fibril-forming motif(s), either over-expressed in

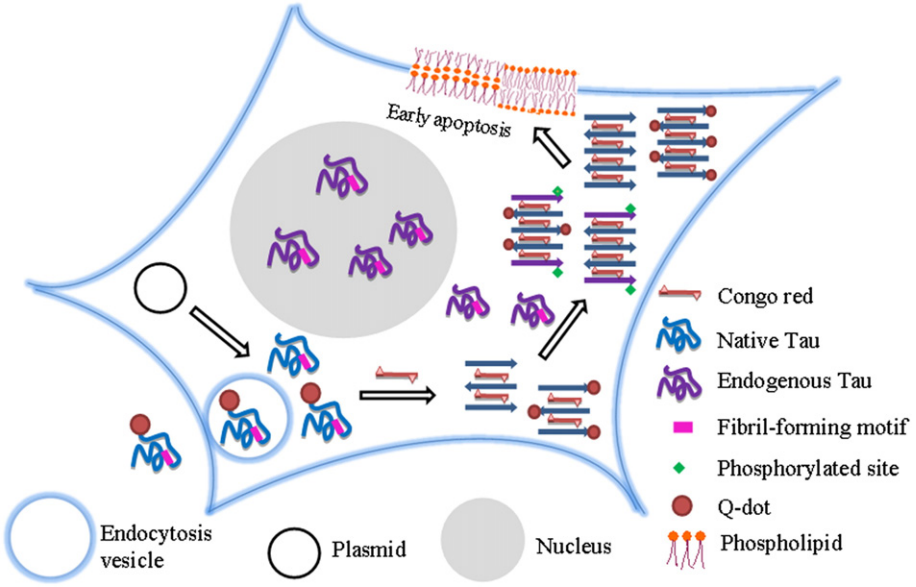


**Fig. 10.** A hypothetical model to explain why fibril-forming motifs are so important for driving human Tau to form fibrils in cells. In the presence of Congo red (red stick), both wild-type $Tau_{244–372}$ and its positive insertion mutant (native Tau monomers, blue), with fibril-forming motifs (pink), either over-expressed in SH-SY5Y cells or marked by quantum dots (red circle) entering into SH-SY5Y cells *via* endocytosis, can form fibrils and enhance hyperphosphorylation of endogenous human Tau (purple; phosphorylation site, green) in SH-SY5Y cells, thereby inducing early apoptosis of living SH-SY5Y cells.

cells or marked by Q-dots entering into cells possibly *via* endocytosis, can form fibrils, thereby inducing early apoptosis of living cells. Therefore, our data provide strong evidence that such a possible endocytosis of human Tau monomers with fibril-forming motif(s) is sufficient to initiate Tau pathology [54,55]. In contrast, none of aggregates and early apoptosis was observed for the double deletion mutant and the negative insertion mutant in living cells. Therefore, insertion of non-fibril forming peptides could be a novel strategy for neurodegenerative disease therapeutics, and fibril-forming units could be molecular bases of prion-like propagation of protein pathology [56]. We claim a link between Tau aggregation and toxicity in the form of apoptosis.

## Author contributions

Planned experiments: YL. Performed experiments: X-LL, J-YH, M-YH, YZ, Z-YH and X-QC. Analyzed the data: X-LL and YL. Contributed reagents/materials: JC and D-WP. Wrote the paper: X-LL and YL.

## Transparency document

The Transparency document associated with this article can be found, in the version.

## Acknowledgements

We sincerely thank Dr. Michel Goedert (University of Cambridge) for kindly providing the human Tau40 plasmid. We thank Dr. Ying Hu and Dr. Li Li in this college and Dr. Zhi-Ping Zhang (Wuhan Institute of Virology, Chinese Academy of Sciences) for their technical assistance on confocal microscope and TEM, respectively. This study was supported by the National Key Basic Research Foundation of China Grants 2013CB910702 and 2012CB911003, National Natural Science Foundation of China Grants 31170744 and 31370774, and Fundamental Research Funds for the Central Universities of China 410500058 and 410500064.

## Appendix A. Supplementary data

Supplementary data to this article can be found online at http://dx.doi.org/10.1016/j.bbadis.2015.04.015.

## References

[1] M. Goedert, M.G. Spillantini, A century of Alzheimer's disease, Science 314 (2006) 777–781.
[2] C. Ballatore, V.M. Lee, J.Q. Trojanowski, Tau-mediated neurodegeneration in Alzheimer's disease and related disorders, Nat. Rev. Neurosci. 8 (2007) 663–672.
[3] H.C. Tai, A. Serrano-Pozo, T. Hashimoto, M.P. Frosch, T.L. Spires-Jones, B.T. Hyman, The synaptic accumulation of hyperphosphorylated Tau oligomers in Alzheimer disease is associated with dysfunction of the ubiquitin–proteasome system, Am. J. Pathol. 181 (2012) 1426–1435.
[4] D. Krstic, I. Knuesel, Deciphering the mechanism underlying late-onset Alzheimer disease, Nat. Rev. Neurol. 9 (2013) 25–34.
[5] V.M. Lee, M. Goedert, J.Q. Trojanowski, Neurodegenerative tauopathies, Annu. Rev. Neurosci. 24 (2001) 1121–1159.
[6] D. Kennedy, C. Norman, What don't we know? Science 309 (2005) 75–102.
[7] B. Frost, R.L. Jacks, M.I. Diamond, Propagation of Tau misfolding from the outside to the inside of a cell, J. Biol. Chem. 284 (2009) 12845–12852.
[8] Z. Zhou, J.B. Fan, H.L. Zhu, F. Shewmaker, X. Yan, X. Chen, J. Chen, G.F. Xiao, L. Guo, Y. Liang, Crowded cell-like environment accelerates the nucleation step of amyloidogenic protein misfolding, J. Biol. Chem. 284 (2009) 30148–30158.
[9] Z.Y. Mo, Y.Z. Zhu, H.L. Zhu, J.B. Fan, J. Chen, Y. Liang, Low micromolar zinc accelerates the fibrillization of human Tau via bridging of Cys-291 and Cys-322, J. Biol. Chem. 284 (2009) 34648–34657.
[10] H.L. Zhu, C. Fernández, J.B. Fan, F. Shewmaker, J. Chen, A.P. Minton, Y. Liang, Quantitative characterization of heparin binding to Tau protein: implication for inducer-mediated Tau filament formation, J. Biol. Chem. 285 (2010) 3592–3599.
[11] J.L. Guo, V.M. Lee, Seeding of normal Tau by pathological Tau conformers drives pathogenesis of Alzheimer-like tangles, J. Biol. Chem. 286 (2011) 15317–15331.
[12] A. de Calignon, M. Polydoro, M. Suárez-Calvet, C. William, D.H. Adamowicz, K.J. Kopeikina, R. Pitstick, N. Sahara, K.H. Ashe, G.A. Carlson, T.L. Spires-Jones, B.T. Hyman, Propagation of Tau pathology in a model of early Alzheimer's disease, Neuron 73 (2012) 685–697.
[13] M.R. Sawaya, S. Sambashivan, R. Nelson, M.I. Ivanova, S.A. Sievers, M.I. Apostol, M.J. Thompson, M. Balbirnie, J.J. Wiltzius, H.T. McFarlane, A.Ø. Madsen, C. Riekel, D. Eisenberg, Atomic structures of amyloid cross-β spines reveal varied steric zippers, Nature 447 (2007) 453–457.
[14] M.I. Ivanova, S.A. Sievers, E.L. Guenther, L.M. Johnson, D.D. Winkler, A. Galaleldeen, M.R. Sawaya, P.J. Hart, D.S. Eisenberg, Aggregation-triggering segments of SOD1 fibril formation support a common pathway for familial and sporadic ALS, Proc. Natl. Acad. Sci. U. S. A. 111 (2014) 197–201.
[15] M.J. Thompson, S.A. Sievers, J. Karanicolas, M.I. Ivanova, D. Baker, D. Eisenberg, The 3D profile method for identifying fibril-forming segments of proteins, Proc. Natl. Acad. Sci. U. S. A. 103 (2006) 4074–4078.
[16] P.K. Teng, D. Eisenberg, Short protein segments can drive a non-fibrillizing protein into the amyloid state, Protein Eng. Des. Sel. 22 (2009) 531–536.
[17] S.A. Sievers, J. Karanicolas, H.W. Chang, A. Zhao, L. Jiang, O. Zirafi, J.T. Stevens, J. Münch, D. Baker, D. Eisenberg, Structure-based design of non-natural amino-acid inhibitors of amyloid fibril formation, Nature 475 (2011) 96–100.
[18] P.N. Cheng, C. Liu, M. Zhao, D. Eisenberg, J.S. Nowick, Amyloid β-sheet mimics that antagonize protein aggregation and reduce amyloid toxicity, Nat. Chem. 4 (2012) 927–933.
[19] S.R. Meng, Y.Z. Zhu, T. Guo, X.L. Liu, J. Chen, Y. Liang, Fibril-forming motifs are essential and sufficient for the fibrillization of human Tau, PLoS One 7 (2012) e38903.
[20] M. von Bergen, P. Friedhoff, J. Biernat, J. Heberle, E.M. Mandelkow, E. Mandelkow, Assembly of Tau protein into Alzheimer paired helical filaments depends on a local sequence motif ($^{306}$VQIVYK$^{311}$) forming β structure, Proc. Natl. Acad. Sci. U. S. A. 97 (2000) 5129–5134.
[21] W. Li, V.M. Lee, Characterization of two VQIXXK motifs for Tau fibrillization in vitro, Biochemistry 45 (2006) 15692–15701.
[22] P. Friedhoff, M. von Bergen, E.M. Mandelkow, P. Davies, E. Mandelkow, A nucleated assembly mechanism of Alzheimer paired helical filaments, Proc. Natl. Acad. Sci. U. S. A. 95 (1998) 15712–15717.
[23] G. Ramachandran, J.B. Udgaonkar, Understanding the kinetic roles of the inducer heparin and of rod-like protofibrils during amyloid fibril formation by Tau protein, J. Biol. Chem. 286 (2011) 38948–38959.
[24] S. Elbaum-Garfinkle, E. Rhoades, Identification of an aggregation-prone structure of Tau, J. Am. Chem. Soc. 134 (2012) 16607–16613.
[25] C.N. Chirita, E.E. Congdon, H. Yin, J. Kuret, Triggers of full-length Tau aggregation: a role for partially folded intermediates, Biochemistry 44 (2005) 5862–5872.
[26] B. Bandyopadhyay, G. Li, H. Yin, J. Kuret, Tau aggregation and toxicity in a cell culture model of tauopathy, J. Biol. Chem. 282 (2007) 16454–16464.
[27] K.I. Lira-De León, P. García-Gutiérrez, I.N. Serratos, M. Palomera-Cárdenas, P. Figueroa-Corona Mdel, V. Campos-Peña, M.A. Meraz-Ríos, Molecular mechanism of Tau aggregation induced by anionic and cationic dyes, J. Alzheimers Dis. 35 (2013) 319–334.
[28] I.L. Medintz, H.T. Uyeda, E.R. Goldman, H. Mattoussi, Quantum dot bioconjugates for imaging, labelling and sensing, Nat. Mater. 4 (2005) 435–446.
[29] X. Michalet, F.F. Pinaud, L.A. Bentolila, J.M. Tsay, S. Doose, J.J. Li, G. Sundaresan, A.M. Wu, S.S. Gambhir, S. Weiss, Quantum dots for live cells, in vivo imaging, and diagnostics, Science 307 (2005) 538–544.
[30] M. Uematsu, E. Adachi, A. Nakamura, K. Tsuchiya, T. Uchihara, Atomic identification of fluorescent Q-dots on Tau-positive fibrils in 3D-reconstructed pick bodies, Am. J. Pathol. 180 (2012) 1394–1397.
[31] M. Chattopadhyay, A. Durazo, S.H. Sohn, C.D. Strong, E.B. Gralla, J.P. Whitelegge, J.S. Valentine, Initiation and elongation in fibrillation of ALS-linked superoxide dismutase, Proc. Natl. Acad. Sci. U. S. A. 105 (2008) 18663–18668.
[32] Z. Zhou, X. Yan, K. Pan, J. Chen, Z.S. Xie, G.F. Xiao, F.Q. Yang, Y. Liang, Fibril formation of the rabbit/human/bovine prion proteins, Biophys. J. 101 (2011) 1483–1492.
[33] E.P. Benditt, N. Eriksen, C. Berglund, Congo red dichroism with dispersed amyloid fibrils, an extrinsic cotton effect, Proc. Natl. Acad. Sci. U. S. A. 66 (1970) 1044–1051.
[34] F. Yang Jr., M. Zhang, B.R. Zhou, J. Chen, Y. Liang, Oleic acid inhibits amyloid formation of the intermediate of α-lactalbumin at moderately acidic pH, J. Mol. Biol. 362 (2006) 821–834.
[35] C. Riccardi, I. Nicoletti, Analysis of apoptosis by propidium iodide staining and flow cytometry, Nat. Protoc. 1 (2006) 1458–1461.
[36] I. Vermes, C. Haanen, H. Steffens-Nakken, C. Reutelingsperger, A novel assay for apoptosis: flow cytometric detection of phosphatidylserine expression on early apoptotic cells using fluorescein labelled annexin V, J. Immunol. Methods 184 (1995) 39–51.
[37] S. Oddo, A. Caccamo, L. Tran, M.P. Lambert, C.G. Glabe, W.L. Klein, F.M. LaFerla, Temporal profile of amyloid-β (A-β) oligomerization in an in vivo model of Alzheimer Disease, J. Biol. Chem. 281 (2006) 1599–1604.
[38] P. Desplats, H.J. Lee, E.J. Bae, C. Patrick, E. Rockenstein, L. Crews, B. Spencer, E. Masliah, S.J. Lee, Inclusion formation and neuronal cell death through neuron-to-neuron transmission of α-synuclein, Proc. Natl. Acad. Sci. U. S. A. 106 (2009) 13010–13015.
[39] C. Münch, J. O'Brien, A. Bertolotti, Prion-like propagation of mutant superoxide dismutase-1 misfolding in neuronal cells, Proc. Natl. Acad. Sci. U. S. A. 108 (2011) 3548–3553.
[40] T. Nonaka, S.T. Watanabe, T. Iwatsubo, M. Hasegawa, Seeded aggregation and toxicity of α-synuclein and Tau, J. Biol. Chem. 285 (2010) 34885–34898.
[41] E.A. Waxman, B.I. Giasson, Induction of intracellular Tau aggregation is promoted by α-synuclein seeds and provides novel insights into the hyperphosphorylation of Tau, J. Neurosci. 31 (2011) 7604–7618.
[42] I. Khlistunova, J. Biernat, Y. Wang, M. Pickhardt, M. von Bergen, Z. Gazova, E. Mandelkow, E.M. Mandelkow, Inducible expression of Tau repeat domain in cell models of tauopathy, J. Biol. Chem. 281 (2006) 1205–1214.

[43] T.J. Cohen, J.L. Guo, D.E. Hurtado, L.K. Kwong, I.P. Mills, J.Q. Trojanowski, V.M. Lee, The acetylation of Tau inhibits its function and promotes pathological Tau aggregation, Nat. Commun. 2 (2011) 252.
[44] Y. Wang, U. Krüger, E. Mandelkow, E.M. Mandelkow, Generation of Tau aggregates and clearance by autophagy in an inducible cell model of tauopathy, Neurodegener. Dis. 7 (2010) 103–107.
[45] P. Frida, S.V. Anisimova, N. Popovicb, Congo red and protein aggregation in neurodegenerative diseases, Brain Res. Rev. 53 (2007) 135–160.
[46] P. Ladewig, Double-refringence of the amyloid–Congo-red-complex in histological sections, Nature 156 (1945) 81–82.
[47] A.K. Schütz, A. Soragni, S. Hornemann, A. Aguzzi, M. Ernst, A. Böckmann, B.H. Meier, The amyloid–Congo red interface at atomic resolution, Angew. Chem. Int. Ed. 50 (2011) 5956–5960.
[48] C. Lendel, C.W. Bertoncin, N. Cremades, C.A. Waudby, M. Vendruscolo, C.M. Dobson, D. Schenk, J. Christodoulou, G. Toth, On the mechanism of nonspecific inhibitors of protein aggregation: dissecting the interactions of α-synuclein with Congo red and lacmoid, Biochemistry 48 (2009) 8322–8334.
[49] Y.S. Kim, T.W. Randolph, M.C. Manning, F.J. Stevens, J.F. Carpenter, Congo red populates partially unfolded states of an amyloidogenic protein to enhance aggregation and amyloid fibril formation, J. Biol. Chem. 278 (2003) 10842–10850.
[50] A. Lorenzo, B.A. Yankner, β-Amyloid neurotoxicity requires fibril formation and is inhibited by Congo red, Proc. Natl. Acad. Sci. U. S. A. 91 (1994) 12243–12247.
[51] R. Demaimay, J. Harper, H. Gordon, D. Weaver, B. Chesebro, B. Caughey, Structural aspects of Congo red as an inhibitor of protease-resistant prion protein formation, J. Neurochem. 71 (1998) 2534–2541.
[52] H. Rudyk, S. Vasiljevic, R.M. Hennion, C.R. Birkett, J. Hope, I.H. Gilbert, Screening Congo red and its analogues for their ability to prevent the formation of PrP-res in scrapie-infected cells, J. Gen. Virol. 81 (2000) 1155–1164.
[53] B. Falcon, A. Cavallini, R. Angers, S. Glover, T.K. Murray, L. Barnham, S. Jackson, M.J. O'Neill, A.M. Isaacs, M.L. Hutton, P.G. Szekeres, M. Goedert, S. Bose, Conformation determines the seeding potencies of native and recombinant Tau aggregates, J. Biol. Chem. 290 (2015) 1049–1065.
[54] C.H. Michel, S. Kumar, D. Pinotsi, A. Tunnacliffe, P. St George-Hyslop, E. Mandelkow, E.M. Mandelkow, C.F. Kaminski, G.S. Kaminski Schierle, Extracellular monomeric Tau protein is sufficient to initiate the spread of Tau protein pathology, J. Biol. Chem. 289 (2014) 956–967.
[55] J.W. Wu, M. Herman, L. Liu, S. Simoes, C.M. Acker, H. Figueroa, J.I. Steinberg, M. Margittai, R. Kayed, C. Zurzolo, G. Di Paolo, K.E. Duff, Small misfolded Tau species are internalized via bulk endocytosis and anterogradely and retrogradely transported in neurons, J. Biol. Chem. 288 (2013) 1856–1870.
[56] B.B. Holmes, M.I. Diamond, Prion-like properties of Tau protein: the importance of extracellular Tau as a therapeutic target, J. Biol. Chem. 289 (2014) 19855–19861.